Supplemental material for "First experimental observation of vacancy assisted martensitic transformation shift in Ni-Fe-Ga alloys"

I. Unzueta,[1,2,*] D. A. Robador-Lorente,[3] E. Cesari,[4] V. Sánchez-Alarcos,[3,5] V. Recarte,[3,5] J. I. Pérez-Landazábal,[3,5] J. A. García,[6,2] and F. Plazaola[1]

[1] *Department of Electricity and Electronics, University of the Basque Country UPV/EHU, 48940 Leioa, Spain*
[2] *BCMaterials, University of Basque Country UPV/EHU, 48940 Leioa, Spain*
[3] *Department of Science, Universidad Pública de Navarra, Campus de Arrosadía, 31006 Pamplona, Spain*
[4] *Department of Physics, Universitat de les Illes Balears, Ctra. de Valldemossa, km 7.5, E-07122, Palma de Mallorca, Spain*
[5] *Institute for Advanced Materials (INAMAT), Universidad Pública de Navarra, Campus de Arrosadía, 31006 Pamplona, Spain*
[6] *Department of Applied Physics II, University of the Basque Country UPV/EHU, 48940 Leioa, Spain*

(Dated: April 2, 2019)

I Experimental details

Starting from high purity elements Ni, Fe and Ga, a polycrystalline ingot was cast by induction melting method under protective Ar atmosphere. The ingot was remelted several times to ensure homogeneity. After encapsulating the ingot in a quartz ampoule it was homogenized during 24 h at 1423 K in Ar atmosphere, followed by slow cooling in the furnace. Composition and the characteristic temperatures T_c and T_{MT} were measured by EDX and DSC respectively in a $Ni_{55}Fe_{17}Ga_{28}$ sample with $T_c \approx T_{MT} \approx 300$ K[1]. The samples studied were quenched in ice water from 673 K to 1173 K in 100 K steps. Samples are labeled according to their quenching temperature T_q as Q673K, Q773K, Q873, Q973 Q1073 and Q1173.

Differential Scanning Calorimetry (DSC) measurements were carried out in a TA-Q100 at a heating/cooling rate of 10 K/min, from which the evolution of the direct T_{MT} was obtained for all samples. These values are gathered in Fig .1.

PALS experiments were performed using a fast-fast timing coincidence spectrometer with a FWHM resolution of 250 ps. The detectors are equipped with plastic scintillators from Saint-Gobain (BC-422) and Hamamatsu photomultiplier tubes (H1949-50) in a collinear geometry. All PALS spectra related to isochronal annealing cycles (IAC) were taken at 350 K (austenite phase, $Fm\bar{3}m$) and the as quenched samples were also measured in the martensite ($I4/mmm$) phase. Spectra were measured using a 15 μCi ^{22}NaCl positron source encapsulated between 7.5 μm Kapton foils and sandwiched by a pair of identical Ni-Fe-Ga samples. Each PALS spectrum was collected with more than 3×10^6 counts and analyzed with the POSITRONFIT code[2].

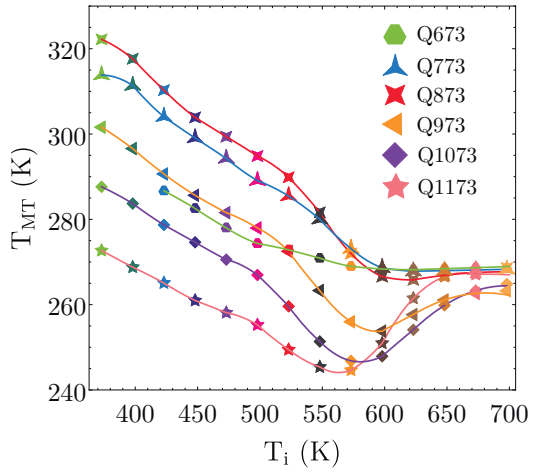

FIG. 1. The evolution of T_{MT} for all samples as a function of T_i.

All spectra were analyzed after subtracting the source contribution, which consists of two components. The lifetime related with the first component is around 1500 ps[3, 4] and the measured intensity was about 1%. The second component is related to the positron annihilation in Kapton which has a well-known value of 382 ps[5, 6]. The intensity of the former component that minimizes the χ^2 in all spectra was %13. In order to improve the accuracy of the PALS measurements, each point was measured up to 6 times. In all the measured points the error of $\overline{\tau}$ has been always below 0.5 ps.

Initially, the $Ni_{55}Fe_{17}Ga_{28}$ sample was slowly cooled from 1173 K, at a cooling rate of 0.3 K/min to 350 K. The sample was then measured by PALS at 350 K (to keep it in austenite phase), revealing an average positron lifetime of 167 ps. This value is lower than the minimum value of $\overline{\tau}$ measured during the isochronal annealing cycles, indicating that thermal vacancies drive the $\overline{\tau}$ variation observed (i. e., C_v).

II. Theoretical calculations of positron lifetimes

Positron lifetime calculations were conducted within the two component density functional theory framework[7, 8]. The annihilation rate λ, which is the inverse of the τ positron lifetime, is evaluated by overlapping the $n_+(\mathbf{r})$ positron and $n_-(\mathbf{r})$ electron

densities of the solid

$$\lambda = \tau^{-1} = \pi c r_o^2 \int n_+(\mathbf{r}) n_-(\mathbf{r}) \gamma(\mathbf{r}) \mathrm{d}\mathbf{r} \quad (1)$$

where c is the speed of light in vacuum, r_0 the classical electron radius and $\gamma(\mathbf{r})$ the so-called enhancement factor that comprises the enhanced electron density due to the Coulombic attraction exerted by e^+. The positron lifetime for the perfect (i. e., bulk lifetime) and defected lattice was computed by the Atomic Superposition Approximation (AT-SUP) method[9]. Within this scheme, the electron density $n_-(\mathbf{r})$, is constructed by adding individual atomic n_-^i charge densities around $\mathbf{R_i}$ atomic positions, over all the occupied atomic sites:

$$n_-(\mathbf{r}) = \sum_i n_-^i(|\mathbf{r} - \mathbf{R_i}|). \quad (2)$$

The potential felt by the positron, $V_+(\mathbf{r})$, is constructed as

$$V_+(\mathbf{r}) = V_c(\mathbf{r}) + V_{corr}[n_-(\mathbf{r})], \quad (3)$$

where $V_c(\mathbf{r})$ is the Coulomb potential of the entire crystal and $V_{corr}[n_-(\mathbf{r})]$ the positron-electron correlation potential, which depends on the electron density.

The enhancement factor of Eq. (1) and the correlation potential of Eq. (3) have been taken into account within *i*) local density approximation (LDA) and *ii*) Generalized Gradient Approximation (GGA) frameworks. Within the LDA approximation, the $V_{corr}[n_-(\mathbf{r})]$ has been modeled using the interpolation formula proposed by Boronski and Nieminen[8], which is based on the results of Arponen and Pajane[10]. Regarding $\gamma(\mathbf{r})$, calculations have been performed by employing three different parameterizations. First, the expression proposed by Boronski and Nieminen[8], which is based on the many-body calculation by Lantto[11] (labeled as LDA-BN),

$$\gamma(\mathbf{r})_{\mathrm{LDA}}^{\mathrm{BN}} = 1 + 1.23 r_s + 0.8295 r_s^{3/2} - 1.26 r_s^2 + 0.3286 r_s^{5/2} + \frac{1}{6} r_s^3 \quad (4)$$

where $r_s = (3/4\pi n_-)^{1/3}$. The other two expressions proposed by Barbiellini *et al.*[12] are based on results of Arponen and Pajanne[10], which have been labeled as LDA-AP1,

$$\gamma(\mathbf{r})_{\mathrm{LDA}}^{\mathrm{AP1}} = 1 + 1.23 r_s - 0.0742 r_s^2 + \frac{1}{6} r_s^3 \quad (5)$$

and LDA-AP2

$$\gamma(\mathbf{r})_{\mathrm{LDA}}^{\mathrm{AP2}} = 1 + 1.23 r_s - 0.91657 r_s^{3/2} + 1.0564 r_s^2 - 0.3455 r_s^{5/2} + \frac{1}{6} r_s^3. \quad (6)$$

respectively. Within the GGA approximation, both correlation energy and the enhancement factors have been taken into account using the expression proposed by Barbiellini *et al.*[12, 13], which is based on the results of Arponen and Pajanne[10]. In this scheme the $\gamma(\mathbf{r})_{\mathrm{GGA}}$ enhancement factor is deduced from the enhancement factor obtained in the LDA scheme. The effects of the non-uniform electron density are modeled by a parameter $\epsilon = |\Delta \ln n_-|^2 / \mathrm{q}_{TF}^2$. It describes the reduction of the screening cloud close to the positron, being q_{TF} the local Thomas-Fermi screening length. Finally, an adjustable parameter α is also introduced so the corrected enhancement factor then reads,

$$\gamma(\mathbf{r})_{\mathrm{GGA}} = 1 + (\gamma(\mathbf{r})_{\mathrm{LDA}} - 1)\, e^{-\alpha\epsilon}. \quad (7)$$

The value of α is set to be $\alpha = 0.22$, which has been proven to give lifetimes for different types of metals and semiconductors in good agreement with the experimental results[12, 14]. For calculations performed within the GGA approximations, two parameterization for the $\gamma(\mathbf{r})_{\mathrm{GGA}}$ of Eq. (7) were used: *i*) the expression of Eq. (5) labeled as $\gamma(\mathbf{r})_{\mathrm{GGA}}^{\mathrm{AP1}}$ and *ii*) the expression of Eq. (6), labeled as $\gamma(\mathbf{r})_{\mathrm{GGA}}^{\mathrm{AP2}}$. It is noteworthy to mention that when $\alpha \to 0$ the Eq. (7) turns into $\gamma(\mathbf{r})_{\mathrm{GGA}} = \gamma(\mathbf{r})_{\mathrm{LDA}}$. $\gamma(\mathbf{r})_{\mathrm{LDA}}^{\mathrm{BN}}$ parameterization gives good account of the experimentally measured lifetimes in the studied Ni-Fe-Ga alloy. However, future works on the implementation of the proposed parameter-free model for $\gamma(\mathbf{r})$[15] and the enhanced electron-positron correlation potential based on quantum Monte Carlo results[16], may shed light on the suitability of other parameterizations for proper lifetime calculations in Ni-Fe-Ga alloys.

The positron lifetime was evaluated at both Γ and L points of the Brillouin zone, as well as calculating the average of the wave functions from Γ and L points. The calculations were performed using the supercell approach accounting for the correct composition of the sample. The supercell corresponding to $Ni_{55}Fe_{17}Ga_{28}$ was built starting from a stoichiometric Ni_2FeGa lattice and by substituting Fe atoms by Ni and Ga atoms[17] until the measured composition of the sample was matched. The antisite atoms were distributed homogeneously. Several configurations of homogeneously distributed antisites were used, giving similar results. Afterwards, in order to overcome artificial defect-defect interactions, caused by periodic boundary conditions, the supercell was built increasing its size in order to ensure the convergence of 0.1 ps in lifetime and 0.01 eV in positron binding energies.

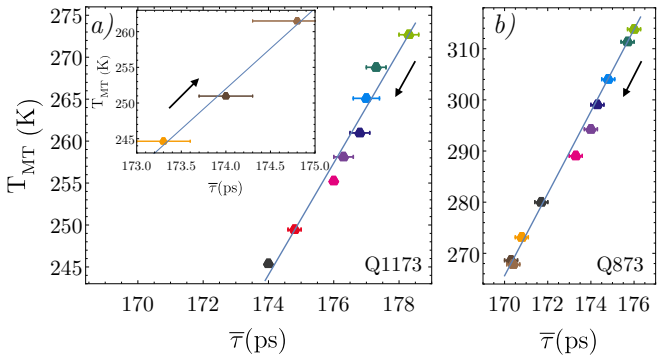

FIG. 2. Mutual relationship between the evolution T_{MT} $\overline{\tau}$ for (a) sample Q1173 and (b) sample Q873.

For the austenite phase a $5 \times 5 \times 5$ supercell expansion of the primitive unit cell[18] was created containing 500 atoms, whereas for the martensite phase a $3 \times 3 \times 3$ supercell expansion of the primitive unit cell[18] has been used with 108 total atoms. A mesh size of 160^3 was used in the austenite and martensite supercells. Finally, the Schrödinger equation is discretized, and the positron wave function and its energy eigenvalue are solved iteratively at the mesh points of the supercell using a numerical relaxation method[19].

II. Relation between the average positron lifetime and vacancy concentration.

Fig. 2 evinces the mutual dependence of the evolution of T_{MT} and C_v. In sample Q1173, the ordering process during subsequent IAC is accomplished by a reduction of $\overline{\tau}$, which in turn, matches with the T_{MT} decrease (see Fig. 2(a)). Additionally, as shown in the inset of Fig. 2(a), between 550 - 600 K, T_{MT} increases with the $\overline{\tau}$ increase, which takes place at same temperature. Regarding the AQ873 sample, Fig. 2(b) shows, again the mutual relationship between the evolution of T_{MT} and $\overline{\tau}$. As it is discussed below, the evolution of $\overline{\tau}$ reflects directly the evolution of C_v.

When a positron enters in a solid, it loses energy until reaches thermal equilibrium. Thermalization is followed by diffusion through the solid, until the positron annihilates with a surrounding electron. In a defect-free lattice, the positron annihilates from the delocalized state (i.e. Bloch state) at an average rate λ_b or with a characteristic lifetime τ_b. However, solids have imperfections in their lattice, such as vacancies, dislocations, etc. that may act as positron traps. The trapping occurs when a positron turns from the Bloch state into a localized state within a defect (i.e. the positron wave function is localized at the defect). The κ_d trapping rate of a defect is proportional to the defect concentration C_d[20] as

$$\kappa_d = \mu_d C_d. \tag{8}$$

The μ_d parameter is the specific trapping coefficient of the defect and it depends on the type of defect and on the surrounding lattice[21, 22].

When a sample contains different positron states (bulk and defect states) where positrons may annihilate, the statistically strongest parameter obtained from PALS spectra is the average positron lifetime $\bar{\tau}$, which is composed by the different positron annihilation contributions coming from the different positron states in the material[23]. The individual η contributions are weighted so that

$$\bar{\tau} = \eta_b \tau_b + \sum_i \eta_v^i \tau_d^i, \tag{9}$$

where τ_d^i is the lifetime related with i-th defect. Vacancies are the most important traps for positrons in metals. Due to the lack of the positive ion, vacancies act as deep traps for positrons. Vacancies are characterized by an open volume with an electron density lower than the one corresponding to the perfect lattice and, as a consequence according to Eq. (1), they exhibit longer positron lifetimes. Beyond open-volume defects, negatively charged defects without open-volume (e.g., acceptor-type impurities or anti-site defects in semiconductors), can also act as shallow positron trapping centers (ST)[24, 25]. In this case, due to the lack of open volume, the wavefunctions of positrons trapped at ST is extended into the bulk surrounding it. Thus, the expected lifetime of positrons trapped in ST is similar to that of the positrons in a Block state or in a delocalized state. Due to the small binding energy of positrons trapped at Rydberg states, the trapping only occurs well below room temperature[26]. Thus, the contribution of anti-site defect and ST centers at room temperature is negligible.

Considering the presence of a single type of open-volume defect, such as a vacancy, ($\kappa_d = \kappa_v, \tau_d = \tau_v$ and $\mu_d = \mu_v$) Eq. (9) adopts the well-known *one-trap model* form,

$$\overline{\tau} = \tau_b \frac{1 + \kappa_v \tau_v}{1 + \kappa_v \tau_b} \tag{10}$$

or,

$$\kappa_v = \mu_v C_v = \frac{1}{\tau_b} \frac{\overline{\tau} - \tau_b}{\tau_v - \overline{\tau}} \quad \rightarrow \quad C_v = \frac{1}{\tau_b \mu_v} \frac{\overline{\tau} - \tau_b}{\tau_v - \overline{\tau}} \tag{11}$$

Eq. (11) evidences the mutual dependency of $\overline{\tau}$ and C_v. Despite that in semiconductors where μ_v may depend on temperature[27], in metals, due to the lack of

charge effects, the specific trapping coefficient has a constant value. Additionally, for a given defect in metals, τ_v remains constant and the value of τ_b is determined by the lattice. As a result, in metals (so in Ni-Fe-Ga) the evolution of $\overline{\tau}$ reflects directly the vacancy dynamics.

The vacancy concentration can be estimated by means of Eq. (11). Usually, τ_v and τ_b can be subtracted after decomposing $\overline{\tau}$. However, this decomposition is not always possible and in the saturation trapping regime ($|\overline{\tau} - \tau_v| < 10$) it is unfeasible to decompose the spectra[23]. However, if the theoretically calculated τ_v and τ_b values are compatible with the experimental results, Eq. (11) can be used to estimate the C_v concentration.

* iraultza.unzueta@ehu.eus

[1] J. M. Barandiarán, V. A. Chernenko, P. Lázpita, J. Gutiérrez, and J. Feuchtwanger, Phys. Rev. B **80**, 104404 (2009).

[2] P. Kirkegaard and M. Eldrup, Comput. Phys. Commun. **7**, 401 (1974).

[3] M. Bertolaccini and L. Zappa, Il Nuovo Cimento B Series 10 **52**, 487 (1967).

[4] B. Somieski, T. Staab, and R. Krause-Rehberg, Nucl. Instrum. Method. A. **381**, 128 (1996).

[5] K. Plotkowski, T. Panek, and J. Kansy, Il Nuovo Cimento D **10**, 933 (1988).

[6] I. MacKenzie and J. Fabian, Il Nuovo Cimento B **58**, 162 (1980).

[7] R. M. Nieminen, E. Boronski, and L. J. Lantto, Phys. Rev. B **32**, 1377 (1985).

[8] E. Boroński and R. M. Nieminen, Phys. Rev. B **34**, 3820 (1986).

[9] M. J. Puska and R. M. Nieminen, J. Phys. F: Met. Phys **13**, 333 (1983).

[10] J. Arponen and E. Pajanne, Ann. Physics **121**, 343 (1979).

[11] L. J. Lantto, Phys. Rev. B **36**, 5160 (1987).

[12] B. Barbiellini, M. J. Puska, T. Torsti, and R. M. Nieminen, Phys. Rev. B **51**, 7341 (1995).

[13] B. Barbiellini, M. J. Puska, T. Korhonen, A. Harju, T. Torsti, and R. M. Nieminen, Phys. Rev. B **53**, 16201 (1996).

[14] J. M. C. Robles, E. Ogando, and F. Plazaola, J. Phys. Condens. Matter **19**, 176222 (2007).

[15] B. Barbiellini and J. Kuriplach, Phys. Rev. Lett. **114**, 147401 (2015).

[16] N. D. Drummond, P. López Ríos, R. J. Needs, and C. J. Pickard, Phys. Rev. Lett. **107**, 207402 (2011).

[17] J. Bai, Y. Chen, Z. Li, P. Jiang, P. Wei, and X. Zhao, AIP Adv. **6**, 125007 (2016).

[18] P. J. Brown, A. P. Gandy, K. Ishida, R. Kainuma, T. Kanomata, H. Morito, K.-U. Neumann, K. Oikawa, and K. R. A. Ziebeck, J. Phys. Condens. Matter **19**, 016201 (2007).

[19] G. E. Kimball and G. H. Shortley, Phys. Rev. **45**, 815 (1934).

[20] W. Brandt and R. Paulin, Phys. Rev. B **5**, 2430 (1972).

[21] P. Hautöjarvi, *Positrons in Solids. Topics in Current Physics*, Vol. 12 (Springer, Heidelberg, 1979).

[22] M. Puska and R. Nieminen, Rev. Mod. Phys. **66**, 841 (1994).

[23] F. Tuomisto and I. Makkonen, Rev. Mod. Phys. **85**, 1583 (2013).

[24] K. Saarinen, P. Hautojärvi, A. Vehanen, R. Krause, and G. Dlubek, Phys. Rev. B **39**, 5287 (1989).

[25] C. Corbel, F. Pierre, K. Saarinen, P. Hautojärvi, and P. Moser, Phys. Rev. B **45**, 3386 (1992).

[26] F. Plazaola, K. Saarinen, L. Dobrzynski, H. Reniewicz, F. Firszt, J. Szatkowski, H. Meczynska, S. Legowski, and S. Chabik, J. Appl. Phys. **88**, 1325 (2000).

[27] R. Krause-Rehberg, A. Polity, W. Siegel, and G. Kuhnel, Semicond. Sci. Tech. **8**, 290 (1993).